USCAP

www.nature.com/labinvest

ARTICLE

Check for updates

SLUG is a key regulator of epithelial-mesenchymal transition in pleomorphic adenoma

Hyesung Kim[1,11], Seung Bum Lee[2,11], Jae Kyung Myung[3,11], Jeong Hwan Park[4], Eunsun Park[1], Dong Il Kim[5], Cheol Lee[6], Younghoon Kim[7], Chul-Min Park[8], Min Bum Kim[9], Gil Chai Lim[10] and Bogun Jang[1]✉

© The Author(s), under exclusive licence to United States and Canadian Academy of Pathology 2022

The histogenesis of pleomorphic adenoma (PA) of the salivary glands remains controversial. PAs are characterized by the transition of epithelial cells to spindled mesenchymal cells, known as epithelial-mesenchymal transition (EMT). The present study aimed to identify a major EMT-inducing transcription factor (EMT-TF) in PAs. Real-time PCR analysis of *SNAIL*, *SLUG*, *ZEB1*, and *TWIST1* demonstrated that only *SLUG* was significantly upregulated in normal salivary glands and PAs. Combined in situ hybridization for *SLUG* and multiplex immunohistochemistry for CK19 and P63 revealed that *SLUG* was specifically expressed in the myoepithelial cells of normal salivary glands. In PAs, *SLUG* was expressed in neoplastic myoepithelial cells and stromal cells but not in the luminal cells lining the inner layers of tumor glands. *SLUG* expression showed no correlation with *PLAG1* expression, and in vitro experiments demonstrated that *PLAG1* suppression in primary cultured PA cells or *PLAG1* overexpression in HEK 293 T cells did not affect *SLUG* levels, indicating that *PLAG1* was not involved in the upregulation of *SLUG* in PAs. The suppression of *SLUG* expression in cultured PA cells resulted in a morphology change to a less elongated shape and attenuated tumor growth. In addition, *SLUG* downregulation led to increased E-cadherin and decreased N-cadherin and vimentin expression levels along with decreased migratory activity in cultured PA cells. These findings suggest that *SLUG* is a major TF that can induce EMT in PAs. In summary, SLUG is specifically and highly expressed in the myoepithelial cells and stromal cells of PAs and is a key regulator of EMT in PAs.

Laboratory Investigation (2022) 102:631–640; https://doi.org/10.1038/s41374-022-00739-1

INTRODUCTION

Pleomorphic adenomas (PAs) are the most common salivary gland neoplasm, accounting for 60% of all epithelial salivary gland tumors[1]. Most PAs originate in the parotid glands; however, they can also arise in the submandibular, sublingual, and minor salivary glands[2]. As benign tumors, PAs are generally presented as a slow growing, asymptomatic mass; however, there is a risk of carcinoma ex PA, a rare carcinoma developing from primary or recurrent PAs[3]. Recurrent translocations or intrachromosomal rearrangements involving *PLAG1* (pleomorphic adenoma gene 1) and *HMGA2* genes are key molecular events in the tumorigenesis of PAs[4]. Multiple *PLAG1* fusion partners have been identified, which include *CTNNB1*, *LIFR*, and *FGFR1*[5]. In addition, two fusion partner genes of *HMGA2* have been identified, i.e., *FHIT* and *NFIB*[6,7]. These fusions result in the ectopic expression of PLAG1 or HMGA2 oncoproteins; thus, immunohistochemistry for PLAG1 and HMGA2 has been suggested as a sensitive diagnostic tool for PAs[8,9].

Histologically, PAs show a highly diverse morphology, typically comprising three components with variable proportions of ductal epithelial, myoepithelial, and stromal cells with a myxoid/chondroid matrix. In particular, neoplastic myoepithelial cells are considered as major proliferating cells in the tumors and responsible for histologic heterogeneity with a wide range of cellular modifications[10]. Myoepithelial cells can give rise to different morphologic cell types such as basaloid cells, epithelioid cells, clear cells, and spindle cells; the majority of PAs exhibit more than one cell type, and different cell types usually mix with each other, forming a continuum with cells in transition[10]. PAs commonly have areas where myoepithelial cells lose adhesion and disperse in copious chondroid/myxoid stroma, which has been recognized as epithelial-mesenchymal transition (EMT)[11,12]. Therefore, it has been suggested that PAs represent an in vivo model of EMT in adult tissues[11]. EMT is a fundamental embryonic process during which polarized epithelial cells convert into motile mesenchymal ones[13]. In addition, EMT has been demonstrated to play important roles in cell invasion, leading to cancer metastasis, and several key transcription factors (TFs) that induce EMT have been identified, including SNAI1/2, TWIST1/2, and ZEB1/2[13]. However, little is known as to which TFs are involved in EMT in PAs.

To the best of our knowledge, only three studies have investigated the expression of EMT-inducing transcription factors (EMT-TFs) in PAs, in which TWIST expression was examined by

[1]Department of Pathology, Jeju National University School of Medicine, Jeju, South Korea. [2]Laboratory of Radiation Exposure and Therapeutics, National Radiation Emergency Medical Center, Korea Institute of Radiological and Medical Science, Seoul, South Korea. [3]Department of Pathology, Hanyang University College of Medicine, Seoul, South Korea. [4]Department of Pathology, SMG-SNU Boramae Medical Center, Seoul, South Korea. [5]Department of Pathology, Green Cross Laboratories, Yongin, Gyeonggi, South Korea. [6]Department of Pathology, Seoul National University College of Medicine, Seoul, South Korea. [7]Laboratory of Epigenetics, Cancer Research Institute, Seoul National University College of Medicine, Seoul, South Korea. [8]Department of Obstetrics & Gynecology, Jeju National University School of Medicine, Jeju, South Korea. [9]Department of Otorhinolaryngology, Jeju National University School of Medicine, Jeju, South Korea. [10]Department of Otorhinolaryngology, Yonsei University College of Medicine, Seoul, South Korea. [11]These authors contributed equally: Hyesung Kim, Seung Bum Lee, Jae Kyung Myung. ✉email: bgjang9633@gmail.com

Received: 7 September 2021 Revised: 15 January 2022 Accepted: 18 January 2022
Published online: 10 February 2022

immunohistochemical or real-time PCR analysis[14–16]. However, they showed inconsistent results. Matsumoto et al. reported negligible levels of TWIST1 in most PAs. In contrast, Shen et al. and Pardis et al. reported 30% and 100% of TWIST1 expression in PAs, respectively. The localization of TWIST1 expression also varied between studies, i.e., nuclear vs. cytoplasmic. Therefore, in this study, we used RNA in situ hybridization (ISH) instead of immunohistochemistry to improve the specificity and sensitivity in detecting the expression of EMT-TFs including *SNAIL*, *SLUG*, *ZEB1*, and *TWIST1* in a series of PAs. In addition, we investigated the correlation between *PLAG1* and *SLUG* expression and the functional roles of *SLUG* in the EMT process using primary cultured PA cells.

MATERIALS AND METHODS

Tissue samples

This study included formalin-fixed and paraffin-embedded (FFPE) PA samples ($n = 28$) that were collected from the patients who underwent surgical resection at Jeju National University Hospital (JNUH) (Jeju, Korea) from 2016 to 2018. Clinicopathological data including age, gender, tumor size, and location were obtained by reviewing pathologic reports (Supplementary Table 1). The classification of cellular subtypes of PAs were determined independently by three pathologists (J.H.P., D.I.K., and C. L.). For primary culture, fresh tumor tissues were obtained from surgical excision material from three patients diagnosed with PA and written informed consent was obtained from the subjects. This study was approved by the Institutional Review Board of JNUH (2019–04–007), and Institutional Review Board confirmed that informed consent for FFPE samples was waived because of the retrospective nature of the study. All procedures were in accordance with the ethical standards of the Helsinki Declaration of 1964 and later versions.

Tissue microarray (TMA) construction

Two TMAs containing 48 tumor cores from 28 PAs (one to two representative cores for each case) were assembled, and normal salivary gland tissues were included in three cores. In brief, through microscopic examination, tumor areas comprising more than 80% of tumor cell population was identified and marked on a hematoxylin and eosin (H&E) slide. Core tissue cylinders with a 4 mm in diameter were punched from individual FFPE specimen of paraffin block and arranged in a new recipient paraffin block using a trephine apparatus (SuperBioChips Laboratories, Seoul, Korea).

Immunohistochemistry and Interpretation

Immunohistochemistry for P63, CK19, E-cadherin, and vimentin were performed on 4 µm TMA sections using a BOND-MAX automated immunostainer and a Bond Polymer Refine Detection kit (Leica Microsystems, Wetzlar, Germany) according to the manufacturer's guidelines. The primary antibodies were anti-P63 (OriGene, Rockville, MD; 1:30), anti-CK19 (BioGenex, San Ramon, CA; 1:500), anti-E-cadherin (BD Biosciences, NJ, 1:800), anti-α-smooth muscle actin (Invitrogen, Carlsbad, CA, 1:1000), anti-calponin 1 (Novus Biologicals, LLC, 1:2000), anti-vimentin (Thermo Fisher Scientific, CA, 1:1500), and anti-PLAG1 (Abnova, Taipei, Taiwan, 1:2000).

RNA extraction from FFPE specimens and real-time PCR

Total RNA was extracted from paraffin-embedded tissue sections with an RNeasy FFPE Kit (Qiagen, Valencia, CA) as previously described[17]. Reverse-transcribed cDNA was prepared from 1 to 2 µg of total RNA with random hexamer primers and the GoScript reverse transcription system (Promega, Madison, WI). Quantitative real-time PCR reactions were performed using Premix EX Taq (Takara Bio, Shiga, Japan) according to the manufacturer's recommendations, and the data analyzed using Sequence Detection System software (Version 1.4, Applied Biosystems). The following TaqMan gene expression assays were used: Hs00195591_m1 (SNAIL), Hs00161904_m1 (SLUG), Hs04989912_s1 (TWIST1), Hs01566408_m1 (ZEB1), Hs00958111_m1 (VIMENTIN), and Hs0275899_g1 (GAPDH). GAPDH served as the endogenous control.

RNA ISH

RNA ISH was performed using RNAscope FFPE assay kit (Advanced Cell Diagnostics, Hayward, CA) as previously described[18]. Briefly, 4 µm FFPE tissue sections are pretreated with heat and protease digestion followed by hybridization with the probe. Then, an HRP-based signal amplification system is hybridized to a probe before color development with 3,3′-diaminobenzeidine tetrahydrochloride (DAB). The housekeeping gene ubiquitin C (UBC) and the bacterial gene DapB served as a positive and negative control, respectively. PA cases with UBC easily visible under a 10× objective lens were considered to be adequate according to the manufacture's recommendation. Positive staining was indicated by brown punctate dots in the nucleus and/or cytoplasm. *SNAIL*, *SLUG*, *TWIST1* and *ZEB1* mRNA expression was quantified according to the manufacturer's scoring guideline: score 0, no staining; score 1: 1–3 dots per cell; score 2: 4–10 dots per cell; score 3: more than 10 dots per cell; score 4: more than 15 dots per cell and >10% positive cells have dot clusters. The histo-scores (H-scores) were calculated as: RNAscope score × % of positive tumor cells, ranging from 0 to 400.

Combined RNA ISH and multiplex IHC

We developed a combined approach of RNA ISH and multiplex IHC by sequentially performing RNA ISH and multiple IHC on identical TMA slides. The process is described as a schematic diagram in Supplementary Fig. 1. Each RNA ISH and IHC procedure was performed in the same manner as described above with the following modifications. First, RNA ISH for *SLUG* was performed, followed by scanning and image acquisition of the whole TMA slide using an Aperio AT2 scanner (Leica Biosystems, Newcastle upon Tyne, UK). The slide was subsequently subjected to IHC for P63 staining. After scanning the newly stained slide, it was treated with stripping buffer (20% sodium dodecyl sulfate, 0.5 M Tris-HCl pH 6.8, β-mercaptoethanol, and distilled water) and microwaved for additional stripping effect. Then, after antigen retrieval, IHC for CK19 staining was performed on the same slide followed by scanning. For analysis, each 4 mm TMA core of the virtual TMA slides was extracted using an Aperio ImageScope (Leica Biosystems). CellProfiler (ver. 3.1.8. Broad Institute, Cambridge, MA) was used to further process the core images. All core images from each staining procedure were converted into grayscale images and each positive expression within the cores were further converted to a specific color; blue for *SLUG*, Red after P63 IHC, and Green after CK19 IHC. For each core, three pseudo-color images representing the three stainings were aligned and merged into a single image. DAB staining of RNA ISH for *SLUG* is irremovable and therefore remains during subsequent IHC and scanning procedures. As a result, *SLUG* expression remains in all three scanned images and appears white when the three color images are merged.

Primary culture of PA cells

Fresh tissue samples were obtained from PAs as previously described[19]. In brief, a tissue slice was minced into small pieces and they were treated with 0.1% (v/w) collagenase (F. Hoffmann-La Roche Ltd., Basel, Switzerland) in Dulbecco's minimal essential medium (DMEM) (Gibco) containing 10% fetal calf serum (Gibco), 50 IU/ml penicillin and 50 µg/ml streptomycin (Gibco) in a 2 ml tube for 8 h at 37 °C. Pass-through fractions from a nylon mesh filter were washed and plated in 2 ml of DMEM in 35 mm dishes and incubated at 37 °C in humidified 5% carbon dioxide/95% air atmosphere. After 2 weeks, culture media were replaced with fresh ones and thereafter changed every 7 days. After one month, the cells were split into 25 cm^2 flasks. When aggregates of polygonal epithelioid cells appeared in the background of spindle-shaped cells in the first passage, the cells were split and thereafter passaged every week.

Immunocytochemistry (ICC)

Cultured PA cells were fixed with 4% paraformaldehyde in PBS for 30 min at room temperature. After washing with PBS, cells were incubated with PBS containing 1% BSA and 0.1% triton X-100 for 1 h at room temperature; this was followed by incubation with primary antibodies including Vimentin (Biovision, California, 1:100), α-SMA (Abcam, Cambridge, MA, cat. No. Ab5694, 1:100), Calponin (Thermo, 1:10,) and CK19 (Dako, Carpinteria, CA, 1:100). Alexa Fluor 594 goat anti-rabbit or mouse IgG (1:500) was used as the secondary antibody. Images were acquired using an immunofluorescence microscope (Olympus Co. Tokyo. Japan).

Transfection

On-Target Plus siRNA pool for PLAG1 and control (On-Target Plus non-targeting siRNA) were purchased from Thermo Fisher Scientific (formerly Dharmacon). PA cells were seeded at 5×10^4 cells/well in six-well plate after transfected with control siRNA or PLAG1 siRNA (100, 200, and 400 pmole) using the Neon transfection system (Thermo Fisher Scientific).

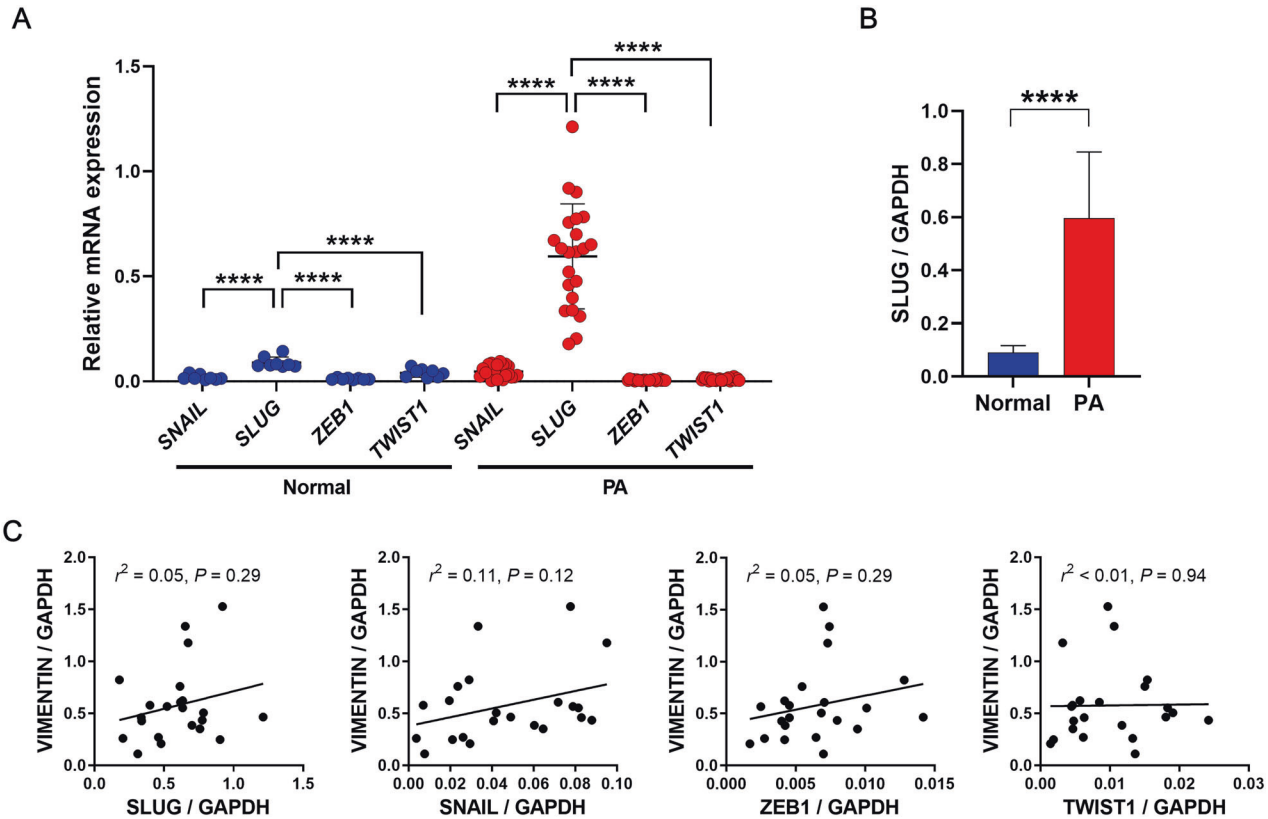

Fig. 1 Expression of epithelial-mesenchymal transition-inducing transcription factors (EMT-TFs) in normal parotid glands and pleomorphic adenomas (PAs). A, **B** Real-time PCR analysis of *SNAIL*, *SLUG*, *ZEB1*, and *TWIST1* was performed with formalin-fixed and paraffin-embedded normal parotid glands ($n = 8$) and PAs ($n = 22$). Among the four EMT-TFs, only *SLUG* was significantly upregulated in the normal tissues and PAs, and it was much higher in PAs than in normal salivary glands. The data are shown as the mean ± SD. **C** Scatter plots revealed no significant correlation between EMT-TF and vimentin expression in PAs. $^{****}P < 0.0001$.

Full-length cDNA encoding PLAG1 (pCMV6-PLAG1) and control vector (pCMV6) were purchased from OriGene (Rockville, MD). HEK 293 T cells were seeded at 1×10^5 cells/well in six-well plate after transfected with control vector or pCMV6-PLAG1 (0.3, 0.6, and 1.2 μg) using the Neon transfection system (Thermo Fisher Scientific). One day or two days after transfection, cells were subjected to real-time PCR. All experiments were performed at least two to three times independently.

Generation of lentivirus and infection of primary cultured PA cells

The lentiviral vectors used in this study were purchased from Addgene (Cambridge, MA; pEGIP, pLKO.1, siSlug1 and siSlug3). We previously described the generation of lentiviral particles[20]. In brief, HEK 293 T cells were seeded and transfected with each lentiviral vector plus the virus packaging plasmid (psPAX2 and pCMV-VSV-G) using Lipofectamine 2000 (Invitrogen). Culture supernatants containing the viruses were harvested 72 h after transfection, filtered and stored at −80 °C degree. For virus infection, cells were seeded in six-well plates. The next day, attached cells were infected with each viral particle. After 6 days, infected cells were used for experiments. To monitor the efficiency of lentivirus infection, the cells transduced with pEGIP lentiviral particle encoding GFP were resuspended in 0.5 ml of FACS buffer (1% BSA in PBS). The efficiency of cell infection was analyzed by FACS using a FACSCanto (BD Biosciences) and the CellQuest program (BD Biosciences).

Cell proliferation assay

Primary cultured cells were seeded at 5×10^4 cells/well into six-well plates and incubated for the indicated days. After trypan blue staining to identify dead cells, the number of live cells was counted using an automated cell counter (Bio-Rad, Hercules, CA). For quantitative analysis of cell proliferation, we also performed MTT assays as previously reported[17]. Briefly, on 6 days, cultured cells were incubated with 10% MTT (AMRESCO, Solon, OH) for 2–3 h at 37 °C. After cell lysis by treatment with 2% sodium dodecyl sulfate and dimethyl sulfoxide, the optical density value of the solution was measured at 562 nm using a Synergy HT (BioTek, Winooski, VT).

RNA preparation and real-time PCR in primary cultured PA cells

Total RNA was prepared from PA cells using an RNase mini kit (Qiagen) according to the manufacturer's protocol. One microgram of RNA was reverse transcribed using an AccuPower RT PreMix kit (Bioneer, Seoul, Korea). Real-time PCR was performed using FastStart Essential DNA Green Master Mix (Roche, Indianapolis, IN). All reactions were performed in triplicate. Primer sequences are listed in Supplementary Table 2.

Migration assay

Migration assay was performed as previously reported[21]. Briefly, transduced cells with lentivirus were seeded in the upper well of a Transwell chamber (8 μm pore size). After 72 h, non–migrated cells on the upper surface of the filter were removed with a cotton swab, and the migrated cells on the lower surface of the filter were fixed and stained with a Kwik-Diff kit (Thermo Fisher Scientific). Migration was determined by counting cells in fields per well, and the extent of migration was expressed as the average number of cells per microscopic field. Cells were imaged by phase contrast microscopy.

Statistical analysis

Statistical analyses were performed using SPPSS software version 18.0 (SPSS, Chicago, IL) and Prism version 9.0.0 (GraphPad Software, San Diego, CA). Between-group comparisons of the real-time PCR data were performed using Student's *t* test or one-way ANOVA with multiple comparisons. Between-group comparisons of H-scores of EMT-TFs, and number of cells (or absorbance) in growth assay were performed using one-way ANOVA with multiple comparisons. The correlations between

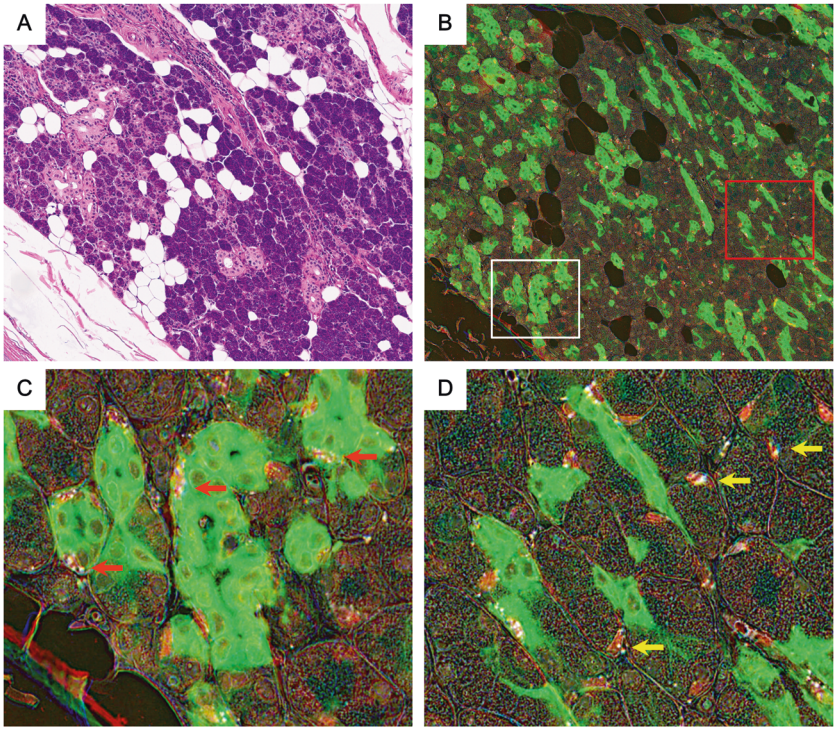

Fig. 2 Combined RNA in situ hybridization for *SLUG* and multiple immunohistochemistry for CK19 and P63 in normal parotid glands. **A** Representative hematoxylin and eosin image of a parotid gland. **B** In situ hybridization for *SLUG* (white dots) and multiplex immunohistochemistry for CK19 (green cytoplasmic stain) and P63 (red nuclear stain) were performed on a single slide. The white and red boxed areas are enlarged in (**C** and **D**), respectively. **C** P63-positive myoepithelial cells around striated and intercalated ducts expressed *SLUG* (red arrows). **D** Myoepithelial cells surrounding acini were also positive for *SLUG* (yellow arrows). Scale bar: 20 μm.

EMT-TFs and vimentin expressions were evaluated by the Spearman correlation test. A P value < 0.05 was considered statistically significant.

RESULTS

Real-time PCR analysis of EMT-TFs in PAs

To identify the TFs involved in EMT in PAs, we first measured the mRNA expression of four EMT-TFs (*SNAIL*, *SLUG*, *TWIST1*, and *ZEB1*) by RT-PCR analysis using FFPE PA samples ($n = 22$) and normal salivary gland tissue samples ($n = 8$). In normal salivary glands, *SLUG* expression was significantly higher than the expression of other TFs ($P < 0.0001$) (Fig. 1A). *SLUG* expression was also significantly elevated compared with the expression of other TFs in PAs ($P < 0.0001$) (Fig. 1A), and the mean *SLUG* level was much higher in PAs than in normal tissues ($P < 0.0001$) (Fig. 1B). As SLUG is one of the major TFs that induce mesenchymal phenotypes, we examined the correlations between EMT-TFs and vimentin; however, no significant association was observed (Fig. 1C).

SLUG expression in the myoepithelial cells of normal salivary glands

To confirm the results of RT-PCR analysis showing *SLUG* expression in normal salivary glands, we performed RNA ISH for four EMT-TFs and found that only *SLUG* was expressed in the salivary glands (Supplementary Figs. 2, 3). RNA ISH for *SLUG* and IHC for α-smooth muscle actin (α-SMA) and P63 on serial sections demonstrated that *SLUG*-positive cells are likely to be myoepithelial cells expressing both α-SMA and P63 (Supplementary Fig. 4). To further confirm this finding, we combined RNA ISH for *SLUG* and multiplex immunohistochemistry for CK19 and P63. In normal salivary glands, which were composed of acini, intercalated ducts, and striated ducts with mixed fatty tissues (Fig. 2A), CK19 stained luminal ductal epithelial cells, and P63 stained myoepithelial cells. Notably, *SLUG* expression was restricted to myoepithelial cells (Fig. 2B–D). Both P63-positive myoepithelial cells around ducts (Fig. 2C) and those surrounding acini (Fig. 2D) showed *SLUG* expression; however, no acinar cells or stromal cells expressed *SLUG*. The expression of *SLUG* in each myoepithelial cell was mostly weak (RNAscope score of 1–2).

Increased *SLUG* expression in the neoplastic myoepithelium in PAs

We performed RNA ISH for four EMT-TFs with tissue microarrays and measured the H-scores of *SLUG* for 28 PAs. Representative images of RNA ISH are shown in Fig. 3A, in which each tumor cell exhibited a high level of *SLUG* expression (RNAscope score of 3–4). In agreement with RT-PCR results, *SLUG* was highly expressed in the majority of PAs; however, the expression of other EMT-TFs was only observed in a few PAs (Fig. 3B). Considering that myoepithelial cells express *SLUG* in normal salivary glands (as demonstrated above) and that neoplastic myoepithelial cells are known to be the major proliferating cells in PAs[10], we measured the percentage of myoepithelial cells by staining for P63 and investigated whether *SLUG* expression is related to the proportion of myoepithelial cells in PAs. Focal Calponin 1 expression confirmed the myoepithelial feature of P63-positive cells. *SLUG* H-scores showed a weak positive correlation with P63 positivity ($P = 0.03$, $r^2 = 0.17$) (Fig. 3C).

The neoplastic myoepithelium shows a wide range of cytologic differentiation features in PAs[10]. To assess the association between the *SLUG* expression and morphologic diversity of myoepithelial cells, we categorized 48 representative spots from 28 PAs into five subtypes based on histologic evaluation and calponin 1 expression: basal/angulated, epithelioid, clear, spindle, and plasmacytoid[10]. The *SLUG* H-scores of spindle cells were higher compared with those of other cell subtypes (Fig. 4). Furthermore, we examined the correlations between *SLUG* and several clinicopathological parameters including patient age,

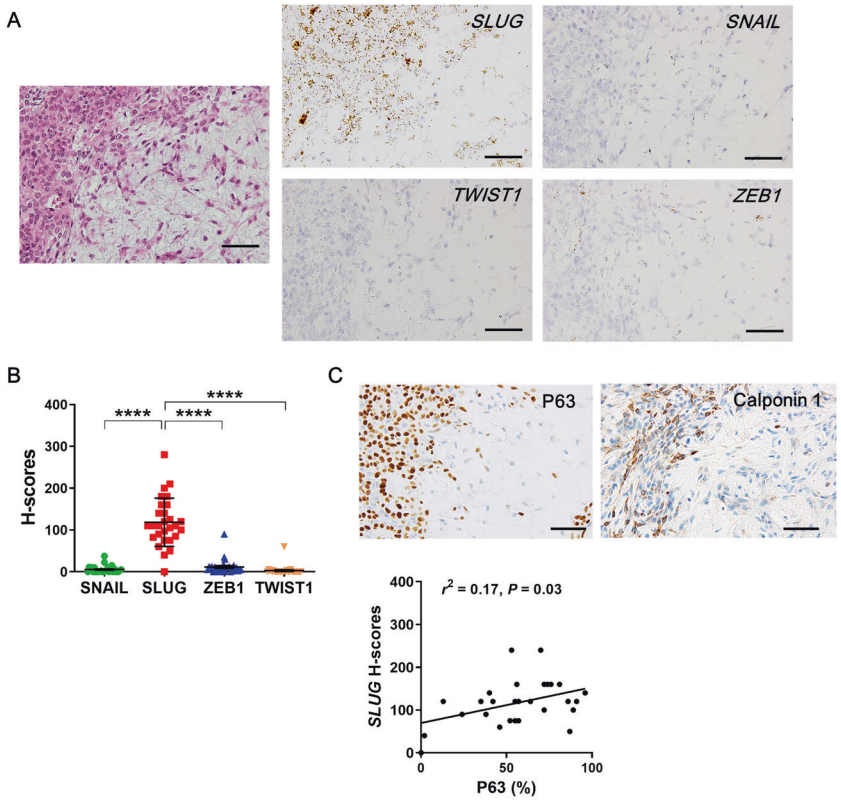

Fig. 3 RNA in situ hybridization for epithelial-mesenchymal transition-inducing transcription factors (EMT-TFs) in pleomorphic adenomas (PAs). A Representative hematoxylin and eosin image of a pleomorphic adenoma exhibiting the transition of epithelial cells to spindled mesenchymal cells and RNA in situ hybridization for *SLUG*, *SNAIL*, *TWIST1*, and *ZEB1*. **B** The Histo-scores (H-scores) of the four EMT-TFs in PAs were determined ($n = 28$). *SLUG* H-scores were much higher than the scores of other EMT-TFs. The data are shown as the mean ± SD. **C** Immunohistochemistry for P63 and calponin 1 identified neoplastic myoepithelial cells in PAs. The scatter plot shows a slight positive correlation between the H-scores of *SLUG* and proportion of P63-positive cells in PAs. Scale bar: 100 μm. $^{****}P < 0.0001$.

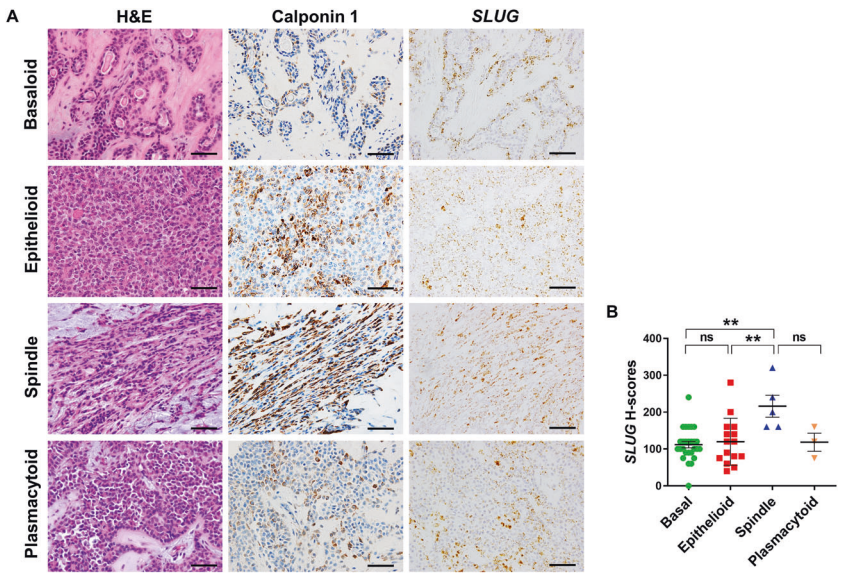

Fig. 4 *SLUG* expression according to cytologic differentiation of myoepithelial cells in pleomorphic adenomas. A Representative images of calponin 1 and *SLUG* expression in each cytologic subtype (basaloid, epithelioid, spindle, and plasmacytoid). **B** The bar graph shows that the histo-scores (H-scores) of *SLUG* were higher in spindle cell areas than in the areas of other cell subtypes ($n = 48$). The data are shown as the mean ± SD. $^{**}P < 0.01$. ns, not significant. Scale bar: 100 μm.

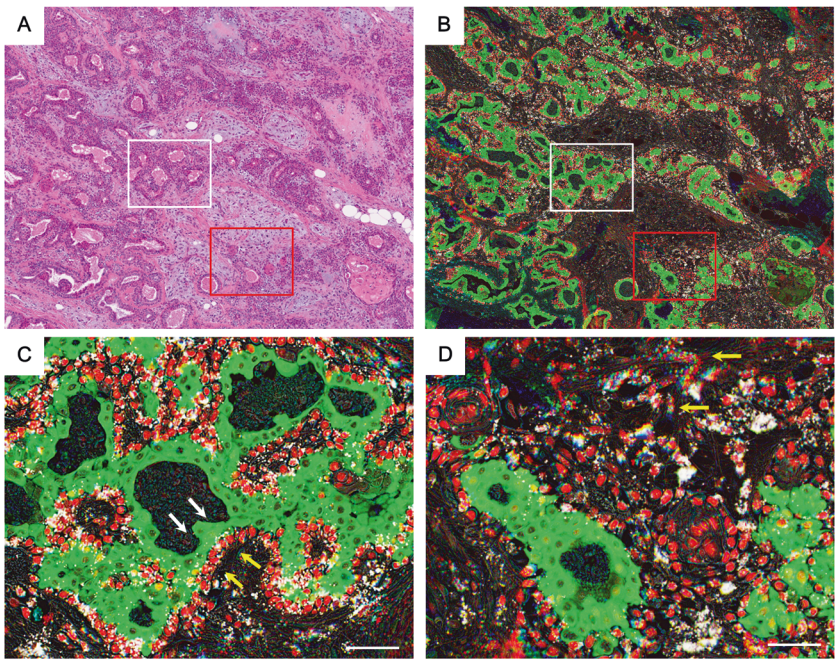

Fig. 5 Combined RNA in situ hybridization for *SLUG* and multiple immunohistochemistry for CK19 and P63 in pleomorphic adenomas. **A** Representative hematoxylin and eosin image of a pleomorphic adenoma. **B** In situ hybridization for *SLUG* (white dots) and immunohistochemistry for CK19 (green cytoplasmic stain) and P63 (red nuclear stain) were performed on a single slide. The white boxed area is enlarged in (**C**), and the red boxed area is enlarged in (**D**). **C** P63-positive neoplastic myoepithelial cells exhibited strong *SLUG* expression (yellow arrows), whereas CK19-positive luminal cells did not express *SLUG* (white arrows). **D** P63-positive neoplastic myoepithelial cells tended to detach from the glands and transform into spindled stromal cells, expressing higher levels of *SLUG* (yellow arrows). Scale bar: 50 μm.

gender, tumor location, tumor size, and metaplasia (Supplementary Fig. 5). However, there was no significant correlation except for the negative correlation of *SLUG* expression with patient age.

Next, we performed RNA ISH for *SLUG* with multiplex immunohistochemistry for CK19 and P63 to identify cells expressing *SLUG* in PAs. As shown in Fig. 5, P63-positive neoplastic myoepithelial and stromal cells exhibited strong *SLUG* expression; however, CK19-positive luminal epithelial cells were negative for *SLUG* (Fig. 5C). In particular, a high level of *SLUG* expression was observed in areas where neoplastic myoepithelial cells tended to lose cohesiveness and detach from the tumor glands (Fig. 5D). Immunohistochemical analysis of additional serial sections demonstrated that *SLUG*-positive myoepithelial cells had significantly decreased E-cadherin expression and weak to moderate vimentin expression, whereas *SLUG*-negative luminal cells had strong E-cadherin expression and no vimentin expression (Fig. 6). The expression profile of EMT markers and histological findings suggest that *SLUG* may be involved in the EMT process in the neoplastic myoepithelial cells of PAs.

PLAG1 and *SLUG* expression in PAs

PAs are known to express high levels of PLAG1 mainly due to the translocation of the *PLAG1* gene, which is considered as a critical event for tumor development. Through RT-PCR analysis with FFPE specimens, we also confirmed the increase in *PLAG1* mRNA expression in PAs compared with normal salivary gland tissues (Fig. 7A); however, there was no significant correlation between *PLAG1* and *SLUG* expression (Fig. 7B). Immunohistochemical analysis for PLAG1 demonstrated diffuse PLAG1 protein expression in most PAs and PLAG1 positivity was also observed in luminal cells in contrast to *SLUG* expression restricted to myoepithelial cells and stromal cells (Fig. 7C). For in vitro analysis of the effect of *PLAG1* on *SLUG* expression, we performed primary culture using three PAs and successfully established one cell line. The PA cell line showed a mixed pattern of epithelial and spindle cells in the first passage, which is a representative histological feature of PAs (Fig. 7D). After three passages, epithelioid cells disappeared and all tumor cells displayed spindle-shaped morphology, and immunocytochemistry demonstrated that they express myoepithelial/mesenchymal markers, but not luminal epithelial markers (Supplementary Fig. 6). We downregulated *PLAG1* expression in the cell line by transfecting the cells with PLAG1-siRNA; however, the reduction of *PLAG1* expression did not result in significant changes in *SLUG* expression (Fig. 7E). Furthermore, the induction of *PLAG1* expression had no effect on *SLUG* expression in H293T cells (Fig. 7F). These results indicated that *PLAG1* may not be involved in the transcriptional regulation of *SLUG* in PA cells.

Association of *SLUG* downregulation with reduced tumor growth and mesenchymal phenotypes in primary cultured PA cells

To determine the functional roles of SLUG as a key regulator of EMT, we downregulated *SLUG* expression by infecting PA cells with lentiviruses expressing *SLUG* shRNAs or control shRNA. RT-PCR analysis revealed that of the two *SLUG*-specific shRNAs (shSLUG#1 and shSLUG#3), only one of them (shSLUG#3) significantly reduced *SLUG* expression compared with the expression in cells infected with pLKO (control shRNA vector) (Fig. 8A). Indeed, shSLUG#3-infected PA cells with reduced *SLUG* expression showed a marked change in morphology to a less elongated cell type (Fig. 8B) and decreased cell growth (Fig. 8C, D). Based on the effects of shSLUG#3, we further evaluated the effect of *SLUG* downregulation on EMT marker expression and migratory activity in PA cells. As expected, following *SLUG* suppression, the expression level of E-cadherin (epithelial marker) was significantly increased, whereas the expression levels of N-cadherin and vimentin (mesenchymal markers) were reduced (Fig. 8E). In agreement with the changes in morphology and EMT markers, the migratory ability of PA cells was reduced when *SLUG* expression was suppressed (Fig. 8F). Taken together, these

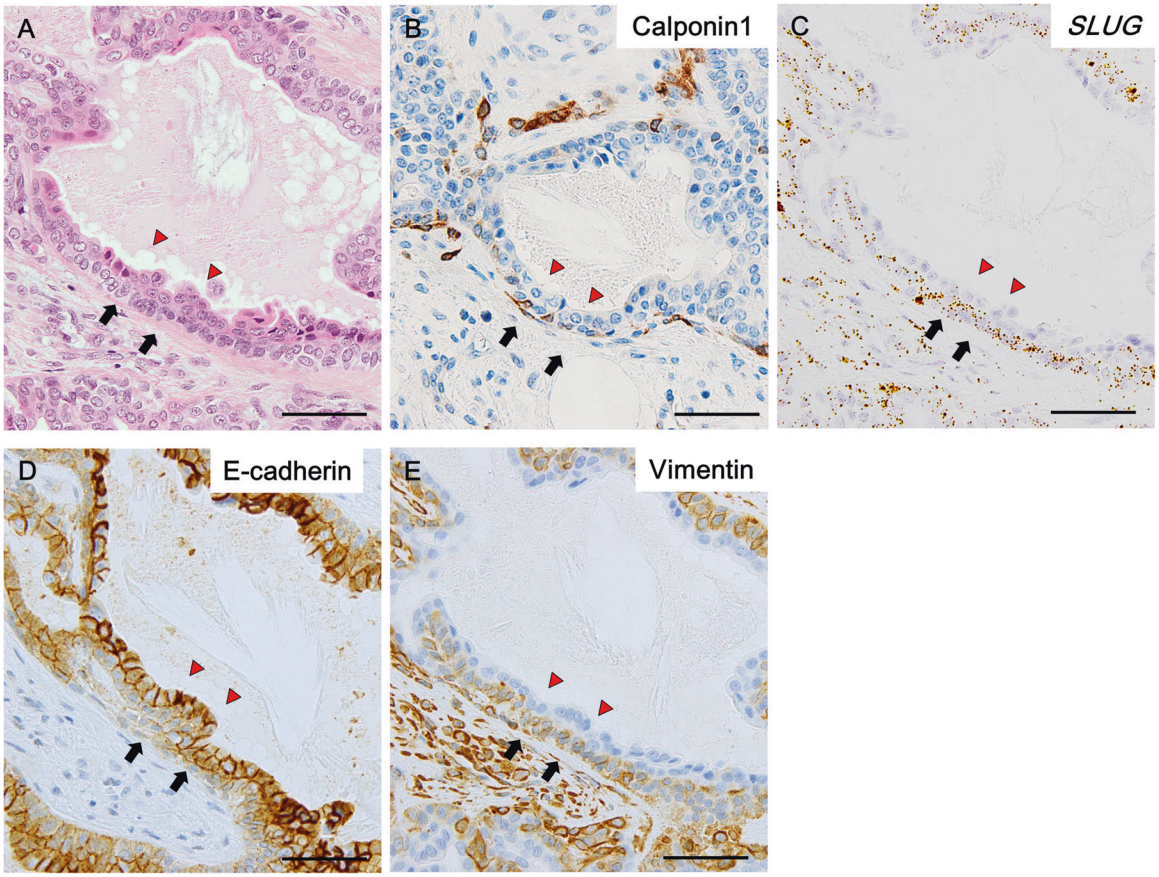

Fig. 6 Correlation between SLUG and epithelial-mesenchymal transition marker expression in pleomorphic adenomas. A Representative hematoxylin and eosin image of a pleomorphic adenoma containing ductal structures composed of luminal cells (red arrow heads) and myoepithelial cells (black arrows). **B** Myoepithelial cells show focal calponin 1 positivity. **C** *SLUG* expression was observed in neoplastic myoepithelial cells and stromal cells but not luminal cells. **D** Luminal cells exhibited strong membranous expression of E-cadherin, whereas myoepithelial cells exhibited a markedly reduced immunoreactivity for E-cadherin. **E** Luminal cells were completely negative for vimentin, whereas myoepithelial cells exhibited weak to moderate immunoreactivity for vimentin. Scale bar: 100 μm.

findings suggest that *SLUG* may play a dual role in PAs, promoting tumor growth and migration while inducing the EMT process.

DISCUSSION

The hallmark of PAs is histologic diversity due to the presence of myoepithelial cells with morphologic plasticity, which may be attributed to EMT. Although some studies have demonstrated the occurrence of EMT within PAs by immunohistochemical and ultrastructural analysis[22–24], specific TFs have not been identified. Here, we examined the expression of four major EMT-TFs and found that *SLUG* was specifically upregulated in PAs, and its expression was restricted to neoplastic myoepithelial cells and stromal cells. Furthermore, using primary cultured PA cells, we found that *SLUG* was involved in tumor growth and regulating EMT marker expression, demonstrating that SLUG is a major TF involved in the EMT process in PAs.

RT-PCR analysis showed low but significant levels of *SLUG* expression in normal salivary glands, in contrast to the negligible levels of *SNAIL*, *ZEB1*, and *TWIST1* expression. RNA ISH also revealed *SLUG*-positive cells that were evenly distributed throughout the salivary glands (Fig. 2). Histological evaluation showed that the *SLUG*-positive cells were slightly oval to spindle-shaped. Given that the normal myoepithelium is wedged between the luminal acinar or ductal cells and the basement membrane, this observation suggests that they may be myoepithelial cells (Supplementary Figs. 2, 3). To verify this, we used a mixed approach by combining RNA ISH for *SLUG* and multiplex immunohistochemistry for CK19 and P63, which allowed us to clearly observe the co-localization of *SLUG* and P63, thus confirming that the myoepithelial cells of salivary glands normally express *SLUG*. These findings led us to speculate that SLUG may be a key TF that confers mesenchymal features such as contractile function and elongated morphology to myoepithelial cells. Myoepithelial cells are known to be present in the mammary, sweat, lacrimal, and mucous glands of the aerodigestive tract and Bartholin's glands[10]. Therefore, it would be interesting to examine the expression of *SLUG* in the myoepithelium of other organs. Indeed, Guo et al. have shown that the Slug protein is specifically expressed in the nuclei of basal cells in the murine mammary epithelium, and Slug and Sox9 act cooperatively to determine the mammary stem cell state[25].

In contrast to cohesive luminal structures, myoepithelial cells begin to separate and disperse into the myxoid stroma at the periphery of tumor glands in PAs (Figs. 3, 5). *SLUG* expression was not observed in luminal epithelial cells (Supplementary Figs. 6, 7), and only *SLUG*-positive myoepithelial cells exhibited changes in EMT markers, i.e., downregulation of E-cadherin and upregulation of N-cadherin and vimentin (Fig. 6). Furthermore, no histological evidence suggesting a direct transition from luminal epithelial cells to stromal cells has been found in PAs. Therefore, we could say that EMT in PAs is technically a transition from myoepithelial cells to mesenchymal cells. However, we cannot rule out the possibility that luminal epithelial cells have the potential to transform into mesenchymal cells. Notably, during the primary culture of PA cells, we could observe cohesive epithelial islands

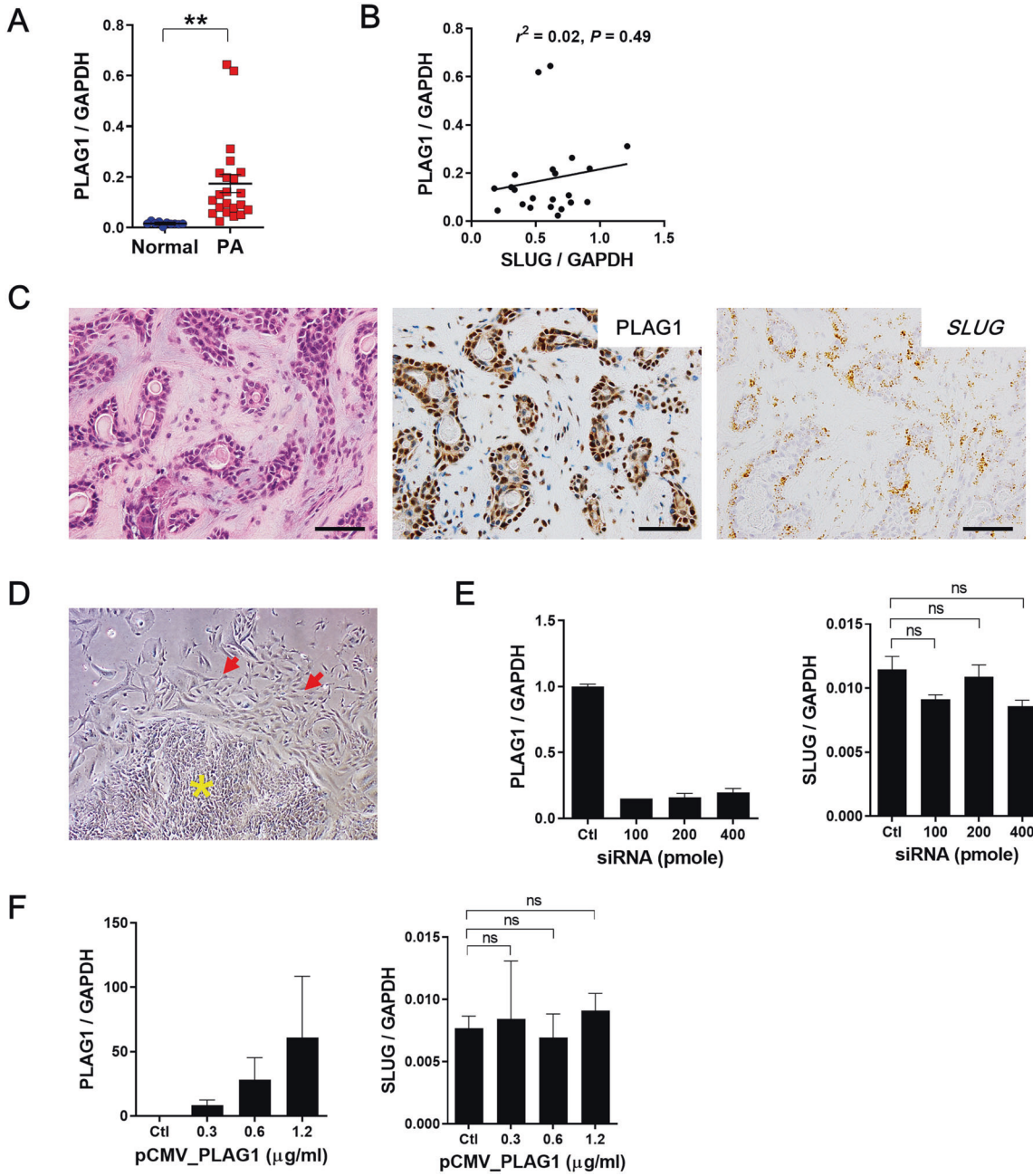

Fig. 7 *SLUG* and *PLAG1* expression in pleomorphic adenomas (PAs). A, **B** Real-time PCR revealed a higher expression of *PLAG1* in PAs ($n = 22$) compared with normal tissues ($n = 10$). There was no correlation between *SLUG* and *PLAG1* mRNA expression. **C** Representative hematoxylin and eosin image of a pleomorphic adenoma expressing PLAG1 and *SLUG*. **D** Primary cultured PA cells exhibited characteristic histological features of PAs (epithelial cell clusters and surrounding spindle cells). **E** *PLAG1* expression was downregulated by transfecting PA cells with PLAG1-siRNA; however, no significant change was detected in *SLUG* expression. **F** *PLAG1* overexpression was induced by transfecting H293T cells with the pCMV6-PLAG1 vector; however, no change was observed in *SLUG* expression. $^{**}P < 0.01$. ns, not significant.

with glandular structures on the first passage (Fig. 7); however, after the second to third passage, all remaining cells were spindle cells. This finding suggests that luminal epithelial cells as well as myoepithelial cells may transform into spindle cells or that luminal cells may not survive under culture conditions in vitro. It remains unclear whether a transition between luminal epithelial cells and myoepithelial cells can occur under certain circumstances in PAs.

Here, we investigated whether *PLAG1* is responsible for *SLUG* overexpression considering that *PLAG1* gene rearrangements are the most common genetic abnormalities in PAs and that PLAG1 as a TF is involved in the regulation of multiple genes such as *IGF2*, *CRABP-II*, *CRP2*, *CLF-1*, and *PIGF*[26]. Moreover, several immunohistochemical studies reported that PLAG1 expression was more prevalent in neoplastic myoepithelial cells[8,27–31], with a similar expression pattern to that of *SLUG*. We hypothesized that *SLUG* might be partly induced by enhanced *PLAG1* expression. However, in vitro analysis using primary cultured PA cells revealed that *PLAG1* had no effect on *SLUG* expression, which is consistent with previous findings. It has been shown that the myoepithelial cells of normal salivary glands do not express PLAG1;[28–30] however, in this study, we found that they express *SLUG*. According to the study by Voz et al., *SLUG* was not on the list of 47 genes consistently and significantly induced by *PLAG1*[26]. Although it appears that *PLAG1* is not directly involved in the transcriptional

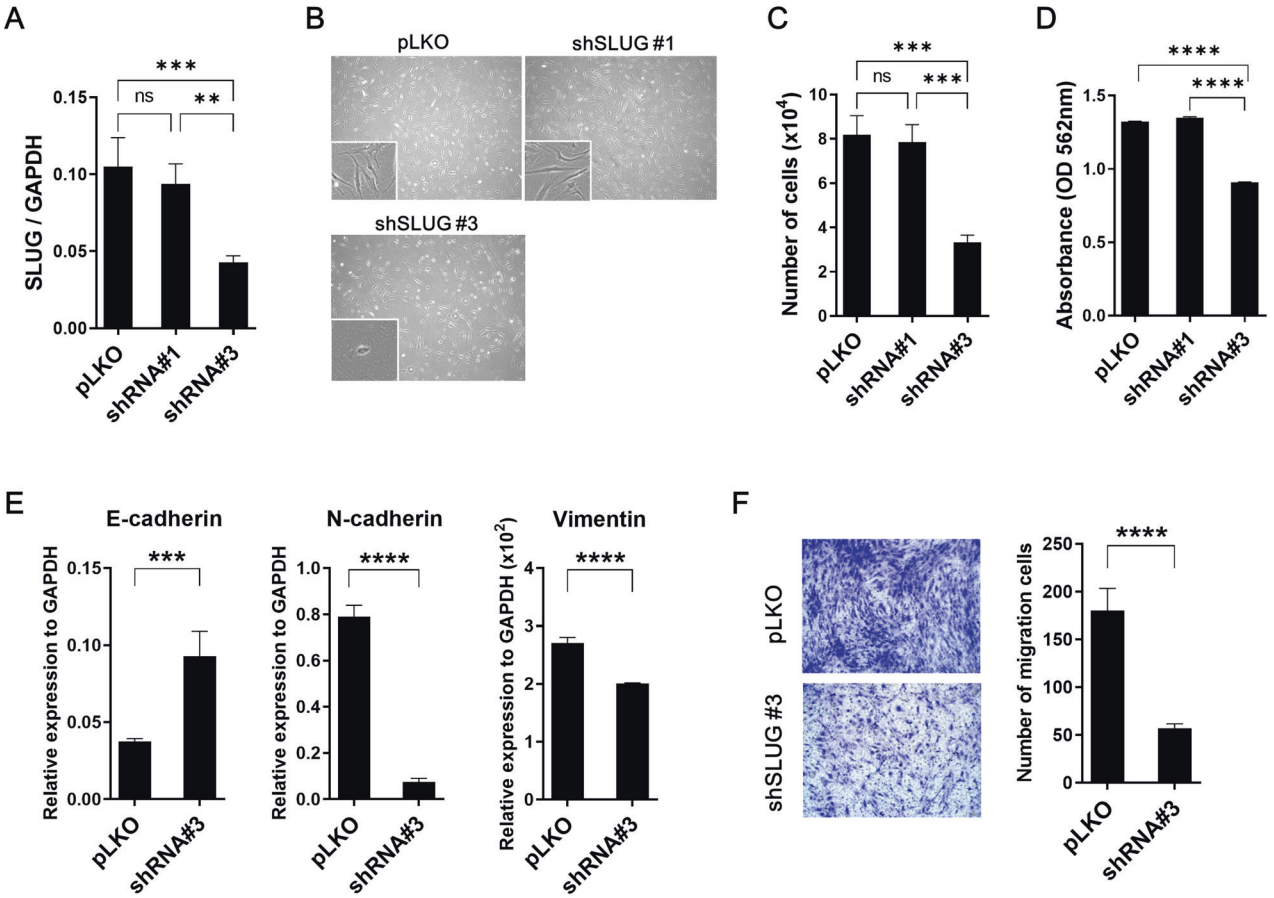

Fig. 8 Association of *SLUG* downregulation with reduced growth and mesenchymal features in primary cultured pleomorphic adenoma (PA) cells. Primary cultured PA cells were infected with the lentiviral-pLKO vector, shSLUG#1, or shSLUG#3. **A** Real-time PCR analysis of *SLUG* was performed using transduced cells on day 6. PA cells transduced with shRNA#3 showed a significant decrease in *SLUG* expression. **B** Images of PA cells taken 3 days after transduction revealed that many PA cells transduced with shSLUG#3 had a round or oval shape. White boxed areas show enlarged images. The growth of transduced PA cells was measured by counting live cells (**C**) or by MTT assays (**D**). **E** PA cells were infected with the lentiviral-pLKO vector or shSLUG#3, and real-time PCR analysis for epithelial-mesenchymal transition markers including E-cadherin, N-cadherin, and vimentin was performed on day 6. **F** The number of migrating cells (pLKO- or shSLUG#3-transduced cells) was quantified. The data are shown as the mean ± SD from triplicate experiments. $^{***}P < 0.001$, $^{****}P < 0.0001$. ns, not significant.

regulation of *SLUG*, there is still the possibility of an intimate cross-talk between the two TFs as they both are well-known to play important roles in the progression of various tumors.

Myoepithelial cells have been reported to consist of tissue-specific stem cells in several organs. For example, in mammary glands, basal myoepithelial cells have been identified as a major cell type that can function as long-lived stem cells with renewal capacity[32–34]. In the trachea, submucosal gland myoepithelial cells function as reserve stem cells that can give rise to the airway surface epithelium as well as submucosal glands[35,36]. Furthermore, in murine salivary glands, Kwak et al. have shown that K14-positive basal/myoepithelial cells in the intercalated ducts represent a long-lived yet cycling population of stem cells that can contribute to the formation and maintenance of the glandular ducts[37]. Considering that tissue-specific stem cells are the cells of origin of tumors, it is reasonable to hypothesize that PAs originate from resident stem cells in the myoepithelium, which normally express low levels of *SLUG*, and *SLUG* expression is upregulated during neoplastic transformation. Further studies are needed to unravel the underlying molecular mechanism for the upregulation of *SLUG* during the development of PAs.

During the primary culture, we found that PA cells grew slowly; their doubling time was ~6 days (Supplementary Fig. 8), which is consistent with their classification as benign tumors. Through transduction with lentiviruses expressing *SLUG*-specific shRNAs, we could suppress *SLUG* expression in PA cells. Notably, *SLUG* downregulation resulted in reduced tumor growth and migratory ability. In addition, we demonstrated that *SLUG* suppression in PA cells led to a morphological change to a less spindled shape and the downregulation of mesenchymal markers, indicating that *SLUG* is responsible for the mesenchymal features of PAs. The findings are consistent with the established functions of *SLUG* in the progression of cancers. To the best of our knowledge, this study is the first to identify SLUG as a major regulator of EMT in tumor progression in PAs. In contrast to carcinoma cells, PAs show easily recognizable histological features associated with EMT; thus, we believe that PAs would be a more appropriate model for future research on EMT in human tumors.

In conclusion, we found that *SLUG* was typically expressed in the myoepithelial cells of salivary glands and was highly upregulated in the neoplastic myoepithelial cells and stromal cells of PAs. *SLUG* expression was slightly higher in spindle cells than in other cell subtypes and was less likely to be affected by *PLAG1*. *SLUG* was involved in the regulation of EMT marker expression in PAs and promoted growth and migration. These findings demonstrated *SLUG* may be a key TF involved in EMT in PAs.

DATA AVAILABILITY

The datasets used and/or analyzed during the current study are available from the corresponding author on reasonable request.

REFERENCES

1. Barnes L., Eveson J., Reichart P., Sidransky D. World Health Organization classifications tumours. *Pathology and genetics of head and neck tumours*. (IARC, 2005).
2. Mendenhall, W. M., Mendenhall, C. M., Werning, J. W., Malyapa, R. S. & Mendenhall, N. P. Salivary gland pleomorphic adenoma. *Am. J. Clin. Oncol.* **31**, 95–99 (2008).
3. Antony, J., Gopalan, V., Smith, R. A. & Lam, A. K. Carcinoma ex pleomorphic adenoma: a comprehensive review of clinical, pathological and molecular data. *Head Neck Pathol.* **6**, 1–9 (2012).
4. Stenman, G. Fusion oncogenes in salivary gland tumors: molecular and clinical consequences. *Head Neck Pathol.* **7**, 12–19 (2013).
5. Kas, K. et al. Promoter swapping between the genes for a novel zinc finger protein and β-catenin in pleiomorphic adenomas with t (3; 8)(p21; q12) translocations. *Nat. Genet.* **15**, 170–174 (1997).
6. Geurts, J. M., Schoenmakers, E. F., Röijer, E., Stenman, G. & Van de Ven, W. J. Expression of reciprocal hybrid transcripts of HMGIC and FHIT in a pleomorphic adenoma of the parotid gland. *Cancer Res.* **57**, 13–17 (1997).
7. Geurts, J. M. et al. Identification of NFIB as recurrent translocation partner gene of HMGIC in pleomorphic adenomas. *Oncogene* **16**, 865–872 (1998).
8. Katabi, N. et al. PLAG1 immunohistochemistry is a sensitive marker for pleomorphic adenoma: a comparative study with PLAG1 genetic abnormalities. *Histopathology* **72**, 285–293 (2018).
9. Mito, J. K., Jo, V. Y., Chiosea, S. I., Dal Cin, P. & Krane, J. F. HMGA 2 is a specific immunohistochemical marker for pleomorphic adenoma and carcinoma ex-pleomorphic adenoma. *Histopathology* **71**, 511–521 (2017).
10. Savera, A. T. & Zarbo, R. J. Defining the role of myoepithelium in salivary gland neoplasia. *Adv. Anat. Pathol.* **11**, 69–85 (2004).
11. Aigner, T., Neureiter, D., Völker, U., Belke, J. & Kirchner, T. Epithelial–mesenchymal transdifferentiation and extracellular matrix gene expression in pleomorphic adenomas of the parotid salivary gland. *J. Pathol.* **186**, 178–185 (1998).
12. Triantafyllou, A. et al. Functional histology of salivary gland pleomorphic adenoma: an appraisal. *Head Neck Pathol.* **9**, 387–404 (2015).
13. Puisieux, A., Brabletz, T. & Caramel, J. Oncogenic roles of EMT-inducing transcription factors. *Nat. Cell Biol.* **16**, 488–494 (2014).
14. Pardis, S., Zare, R., Jaafari-Ashkavandi, Z., Ashraf, M. J. & Khademi, B. Twist expression in pleomorphic adenoma, adenoid cystic carcinoma and mucoepidermoid carcinoma of salivary glands. *Turk. Patoloji Derg.* **32**, 15–21 (2016).
15. Matsumoto, Y. et al. Transcription factors related to chondrogenesis in pleomorphic adenoma of the salivary gland: a mechanism of mesenchymal tissue formation. *Lab. Investig.* **96**, 16–24 (2016).
16. Shen, M., Wen, Y., Hua, C. & Xiao, J. The expression of Twist in salivary adenoid cystic carcinoma and its clinicopathological significance. *Chin. J. Clin. Oncol.* **9**, 187–192 (2010).
17. Kim, Y. H. et al. Evaluation of the radiation response and regenerative effects of mesenchymal stem cell-conditioned medium in an intestinal organoid system. *Biotechnol. Bioeng.* **117**, 3639–3650 (2020).
18. Jang, B. G. et al. Expression profile of LGR5 and its prognostic significance in colorectal cancer progression. *Am. J. Pathol.* **188**, 2236–2250 (2018).
19. Maruyama, S. et al. Establishment and characterization of pleomorphic adenoma cell systems: an in-vitro demonstration of carcinomas arising secondarily from adenomas in the salivary gland. *BMC Cancer* **9**, 247 (2009).
20. Kim, Y. et al. Small molecule-mediated reprogramming of human hepatocytes into bipotent progenitor cells. *J. Hepatol.* **70**, 97–107 (2019).
21. Park, J. H. et al. Radiation-Activated PI3K/AKT Pathway Promotes the Induction of Cancer Stem-Like Cells via the Upregulation of SOX2 in Colorectal. *Cancer. Cells* **10**, 135 (2021).
22. Kusafuka, K., Yamaguchi, A., Kayano, T. & Takemura, T. Immunohistochemical localization of members of the transforming growth factor (TGF)-β superfamily in normal human salivary glands and pleomorphic adenomas. *J. Oral Pathol. Med.* **30**, 413–420 (2001).
23. Enescu, A., Enescu, A. Ş., Florou, C. & Petrescu, F. E-cadherin and α-SMA expression in the epithelial-mesenchymal transition of salivary glands pleomorphic adenomas. *Rom. J. Morphol. Embryol.* **55**, 1383–1387 (2014).
24. Devi A., et al. Potential immmunohistochemical markers to characterize epithelialmesenchymal transition in pleomorphic adenoma. *J. Exp. Ther. Oncol.* **13**, 1–7 (2019).
25. Guo, W. et al. Slug and Sox9 cooperatively determine the mammary stem cell state. *Cell* **148**, 1015–1028 (2012).
26. Voz, M. L. et al. Microarray screening for target genes of the proto-oncogene PLAG1. *Oncogene* **23**, 179–191 (2004).
27. de Brito, B. S. et al. Loss of expression of Plag1 in malignant transformation from pleomorphic adenoma to carcinoma ex pleomorphic adenoma. *Hum. Pathol.* **57**, 152–159 (2016).
28. Rotellini, M., Palomba, A., Baroni, G. & Franchi, A. Diagnostic utility of PLAG1 immunohistochemical determination in salivary gland tumors. *Appl. Immunohistochem. Mol. Morphol.* **22**, 390–394 (2014).
29. Debiec-Rychter, M. et al. Histologic localization of PLAG1 (pleomorphic adenoma gene 1) in pleomorphic adenoma of the salivary gland: cytogenetic evidence of common origin of phenotypically diverse cells. *Lab. Investig.* **81**, 1289–1297 (2001).
30. Lee, J. H. et al. PLAG1, SOX10, and Myb expression in benign and malignant salivary gland neoplasms. *J. Pathol. Transl. Med.* **53**, 23 (2019).
31. Matsuyama, A., Hisaoka, M., Nagao, Y. & Hashimoto, H. Aberrant PLAG1 expression in pleomorphic adenomas of the salivary gland: a molecular genetic and immunohistochemical study. *Virchows Arch.* **458**, 583–592 (2011).
32. Van Keymeulen, A. et al. Distinct stem cells contribute to mammary gland development and maintenance. *Nature* **479**, 189–193 (2011).
33. Plaks, V. et al. Lgr5-expressing cells are sufficient and necessary for postnatal mammary gland organogenesis. *Cell Rep.* **3**, 70–78 (2013).
34. Prater, M. D. et al. Mammary stem cells have myoepithelial cell properties. *Nat. Cell Biol.* **16**, 942–950 (2014).
35. Tata, A. et al. Myoepithelial cells of submucosal glands can function as reserve stem cells to regenerate airways after injury. *Cell Stem Cell* **22**, 668–683. e666 (2018).
36. Lynch, T. J. et al. Submucosal gland myoepithelial cells are reserve stem cells that can regenerate mouse tracheal epithelium. *Cell Stem Cell* **22**, 653–667. e655 (2018).
37. Kwak, M., Alston, N. & Ghazizadeh, S. Identification of stem cells in the secretory complex of salivary glands. *J. Dent. Res.* **95**, 776–783 (2016).

ACKNOWLEDGEMENTS

We sincerely appreciate Professor Woo Ho Kim of Superbiochips for his help with the combined RNA in situ hybridization and immunohistochemical analysis.

AUTHOR CONTRIBUTIONS

H.K., S.B.L., and J.K.M. performed the experiments and drafted the paper. C.M.P., G.C. L., and M.B.K. contributed to data collection. J.H.P., D.I.K., E.P., and C.L. provided interpretation of data. Y.K. provided data analysis and interpretation of RNA in situ hybridization and immunohistochemistry. B.J. designed the study, supervised the experiments, and reviewed the paper. All authors read and approved the final paper.

FUNDING

This research was supported by the Bio & Medical Technology Development Program of the National Research Foundation (NRF) funded by the Korean government (MSIT) (No. 2021R1C1C1011172) (to B.J.), (NO. 2020R1I1A1A01069168) (to H.K.) and research fund of Hanyang University (HY-202000000002704) (to J.K.M).

COMPETING INTERESTS

The authors declare no competing interests.

ETHICS APPROVAL

This study was approved by the Institutional Review Board of JNUH (2019–04–007). Institutional Review Board confirmed that informed consent for FFPE samples was waived because of the retrospective nature of the study, while informed consent was obtained for the primary culture of PA cells. All procedures were in accordance with the ethical standards of the Helsinki Declaration of 1964 and later versions.

ADDITIONAL INFORMATION

Supplementary information The online version contains supplementary material available at https://doi.org/10.1038/s41374-022-00739-1.

Correspondence and requests for materials should be addressed to Bogun Jang.

Reprints and permission information is available at http://www.nature.com/reprints

Publisher's note Springer Nature remains neutral with regard to jurisdictional claims in published maps and institutional affiliations.